Journal of Sound and Vibration (1983) **86**(4), 475–483

TURBULENCE MEASUREMENTS IN A RESONANCE TUBE

K. H. CHOU

Department of Mechanical Engineering, Texas A & M University, College Station, Texas 77843, *U.S.A.*

AND

P. S. LEE AND D. T. SHAW

Laboratory for Power and Environmental Studies, State University of New York at Buffalo, Amherst, New York 14226, *U.S.A.*

(*Received* 14 *February* 1980, *and in revised form* 28 *May* 1982)

Experimental investigations of acoustically induced turbulence in a resonance tube have been performed. Frequency (f) and sound pressure level (I_p) effects have been studied. Measurements were made at various spatial locations on loops and nodes. Sampled data were processed to estimate the characteristics of turbulence. It is found that the acoustically induced turbulence appears when I_p exceeds 160 dB under the experimental conditions of $f = 680$–2740 Hz and $I_p = 160$–166 dB. The turbulent spectrum (F) and the wave number (k) are found to satisfy a power law $F \propto K^s$ with $s \simeq -1{\cdot}6$ to $-2{\cdot}1$. The r.m.s. turbulent velocity ($\tilde{u}$) is experimentally found to have an $I_p^{1/2}$ dependence, yet is relatively insensitive to the variation of f. Throughout the whole measuring range of f and I_p, the rate of energy dissipation per unit mass (ε) is estimated to be in the order of 10^6–10^7 cm^2/s^3.

1. INTRODUCTION

The propagation of a high intensity acoustic wave is accompanied by a whole series of non-linear effects [1]. In a resonance tube, at a high applied sound pressure level, it is noteworthy that a transition to turbulence is possible [2, 3]. Furthermore, traveling shock waves will appear inside the tube if the operating frequency falls within a narrow band around the resonance frequencies [4–7]. Physically, although acoustic turbulence itself may be weak while accompanied by the appearance of the formation of the shock waves, it must be strong turbulence because shocks are always associated with very strong wave–wave interactions. No experiment concerned with the characteristics of such turbulence when it appears in a resonance tube has been previously reported. In this paper we report such an experimental investigation with special emphasis on the frequency (f) and sound pressure level (I_p) effects of the applied acoustic field. In addition, the time rate of energy dissipation (ε) of the turbulence and the Kolmogorov scales of length (η) and time (τ) are estimated (a list of symbols is given in the Appendix).

2. EXPERIMENTAL ARRANGEMENT

In the experimental investigation an acoustic driving system capable of producing a standing wave with I_p up to 166 dB at nodes was used. This driving system consists of a University Sound ID-75 driver assembly, a Hewlett Packard 205A signal generator and a Strom 300 watt power amplifier. In addition, a flow velocity measuring system

0022–460X/83/040475+09 $03.00/0

(TSI 1210-20 hot film probe, TSI 1210 T1.5 hot wire probe and TSI 1050 series thermal anemometer system), for both the acoustic velocity and turbulence measurements, an acoustic pressure measuring system (1/4 in Brüel and Kjaer condenser microphone, and 2121 sound level meter), which measures the acoustic intensity up to 166 dB with an accuracy of ±0·5 dB, and a wide band signal processing system (Norland 3001 processing digital oscilloscope, 3701R floppy disk permanent storage system, and a 3106 CRT Monitor) were used.

The experimental apparatus and instrumentation are shown schematically in Figure 1. The Plexiglass test tube (5 ft long and 3 in diameter) was sealed by a 1/2 in thick

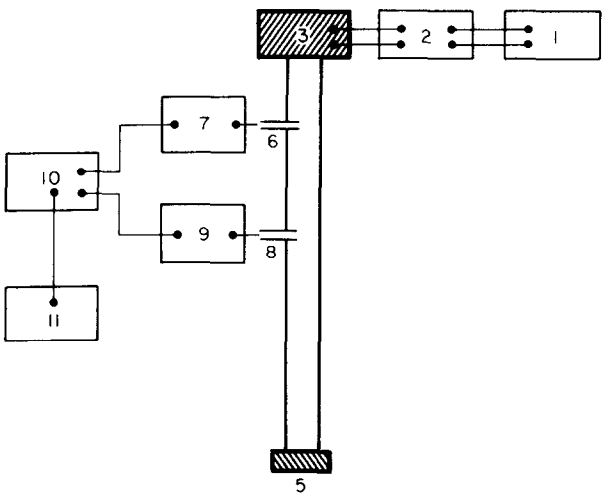

Figure 1. Schematic diagram of the experimental set-up. One-quarter inch Brüel and Kjaer (B & K) condenser microphone (6), TSI 1210-20 hot film probe (8) and TSI 1210-TI.5 hot wire probe are separately inserted into the tube at different locations. The operation ranges of I_p and f are 160–166 dB and 680–2740 Hz, respectively. 1, HP-205A signal generator; 2, Strom 300 watt power amplifier; 3, University Sound ID-75 driver; 4, Plexiglass test tube; 5, bottom plate; 6, 1/4 in B & K condenser microphone; 7, B & K 2121 sound level meter; 8, TSI 1210-20 hot film probe; TSI 1210-T1.5 hot wire probe; 9, TSI 1050 serial thermal anemometer system; 10, Norland 3001 processing digital oscilloscope; 11, 3701R flexible disk permanent storage system.

aluminum plate at the bottom and the top was joined with an assembly of drivers which were powered by a sine wave generator combined with a power amplifier. Since the hot wire probe would possibly pick up the tube vibration, foam materials were used to prevent transmission of driver vibration to the test tube. Failure to do so would change the characteristics of the turbulent spectra because of the presence of a single sharp peak in the spectra due to the probe vibration. In the experiments, I_p could be chosen in the range 151–166 dB, with resonance frequency of 680 Hz. Both the microphone and hot film probe were placed at different locations for measurements. The output signal was converted through an A/D converter and stored in the floppy disk for processing. Statistical parameters, such as r.m.s. value, autocorrelation, and power spectral density, were estimated. The detailed step-by-step measuring procedures are illustrated in the next section.

3. EXPERIMENTAL MEASUREMENTS

In the experiments the hot film probe was inserted into the test tube to measure acoustically induced turbulence and shock on both loop and node. By means of square

wave testing its cut-off frequency for 3 dB attenuation of closed loop response was ultimately calibrated to be approximately 18 kHz. The signal to noise ratio and stability were also adjusted to optimize the performance. The probe support was well sealed by silicon rubber to prevent air leakage and radial movement of the probe. An operating frequency of $f_0 = 695$ Hz was selected to coincide with a resonance condition in the test tube. A standing wave ratio of 7 was best achieved. Figure 2(a) shows the signals taken at loop as the I_p rises. After I_p reaches a certain threshold value (~160 dB), the turbulent bursts in the hot film measurement are shown in Figures 2(b) and (c), in which all the signals were sampled at intervals of 2 seconds. The time-varying waveforms confirm that the turbulent bursts were random signals. On the other hand, the dashed line parts of the waveforms shown in Figures 2(b) and (c) can be regarded as indications of shock response. In addition, the microphone measurements at the different spatial locations, node, quarter point, and loop, are shown in Figure 2(d). The pressure signals at these spatial locations can be seen to have one discontinuity per period at a node, two discontinuities at a loop, and one discontinuity riding on the other at the quarter wave point.

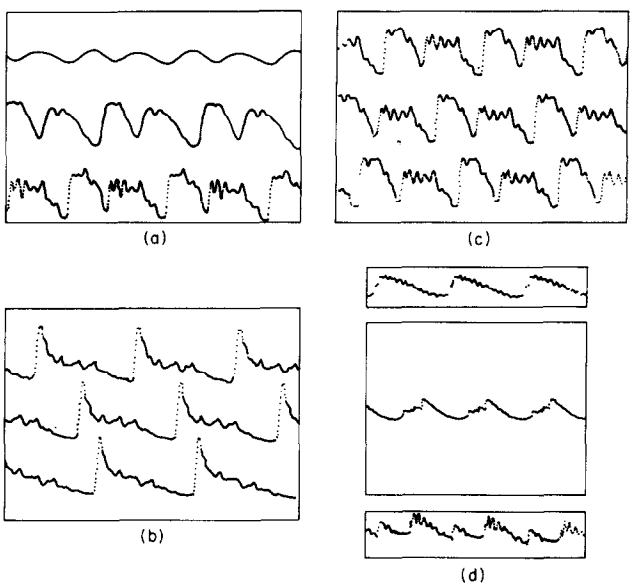

Figure 2. Hot film and microphone signals. (a) Hot film signals at a loop, for $f = f_0$, at various I_p; from top to bottom, $I_p < 160$ dB, $I_p = 161$ dB and $I_p = 166$ dB; these waveforms show the waveform distribution and the appearance of turbulence and shock waves; (b) hot film signal at a node, for $f = f_0$, $I_p = 166$ dB; (c) hot film signals at a loop, for $f = f_0$, $I_p = 166$ dB; two shock waves per period are clearly shown in these signals.

Subsequent operating frequencies were altered to f_0, $2f_0$, $3f_0$, and $4f_0$, with I_p at the node remaining at 166 dB. The results revealed that the turbulent bursts consistently appeared in all measurements. For comparison a traveling wave was set up in a test tube with maximum I_p at 156 dB; measurements of signal, spectrum and autocorrelation shown in Figure 3 indicate no transition to turbulence.

In measurements of the internal structure of the acoustically induced turbulence (e.g., the integral scale, Taylor's microscale, autocorrelation, power spectral density and energy dissipation rate) and its relationship to the physical parameters of the acoustic field in terms of spatial location, frequency and sound pressure level were studied in detail in a set of experiments.

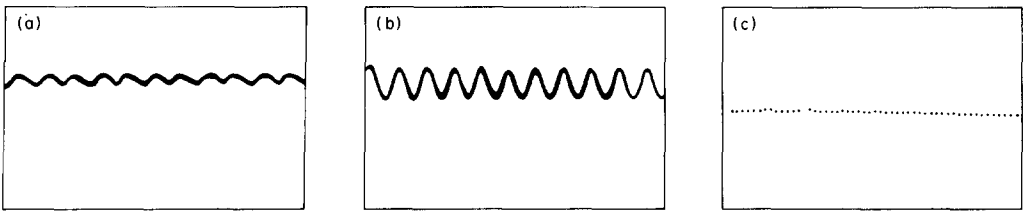

Figure 3. Hot film signal of traveling wave. $I_p = 156$ dB, $f = 1{\cdot}25$ kHz. (a) Wave form; (b) autocorrelation; (c) spectrum.

The hot film probe was firmly placed at different locations by using a wire micromanipulator (i.e., node edge, node center, loop edge and loop center). The waveforms of the signals were first displayed on a CRT display monitor and then picked up by using a processing digital oscilloscope in the manual hold mode, with external sample pulses. As the standing wave was tuned up, the output of the constant temperature anemometer was sampled and each sample was recorded through a memory quadrant. Finally, all the sampled signals were stored in files on the floppy disk for data processing.

A single, complete cycle waveform signal could be analyzed, or a number of them collected and averaged. Since the process was stationary, the time averages and ensemble averages should be equivalent according to the ergodic hypothesis; thus records of length of 1024 collections were sampled at the rate of 5 μs to find the time average. The averaging technique provided improvement of the signal to noise ratio and smoothing of fluctuations from one sample to the other.

Provided the turbulent bursts and the waveforms of the oscillational velocity were statistically independent, autocorrelation and power spectral density of both portions of the signal could be treated as additive quantities. Because of the low level turbulent intensity in these experiments the required information of the low level turbulent intensity in these experiments the required information of turbulence is suppressed when the whole waveform is processed (see Figure 4). Thus, it is necessary to condition the

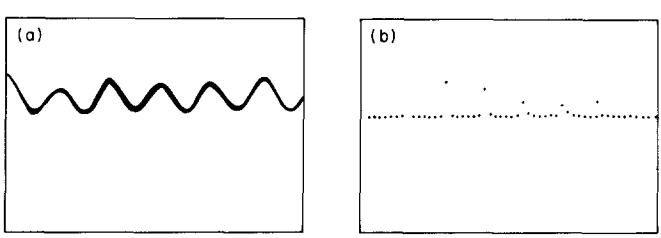

Figure 4. Autocorrelation and total spectrum of hot film signal at $f = f_0$ and $I_p = 166$ dB. (a) Autocorrelation; (b) total spectrum. Information of turbulence is suppressed if complete waveform is processed. This indicates the necessity of signal conditioning.

waveform of the signals and separate the turbulent bursts for analysis. A computer program was developed for this purpose. After conditioning, the turbulent burst was separated from the whole waveform of the signal as shown in Figures 5(a) and (d).

After the waveform was conditioned, the r.m.s. values of the conditioned signal and its time derivative were recorded for estimating Taylor's microscale and the time-lag between zero-crossings of the conditioned signal was also recorded to check this estimation. Autocorrelation of the conditioned signal was also performed. Finally, fast Fourier transform of the autocorrelation provided information on the power spectral density (see Figures 5(b), (c), (e), and (f) on both loop and node).

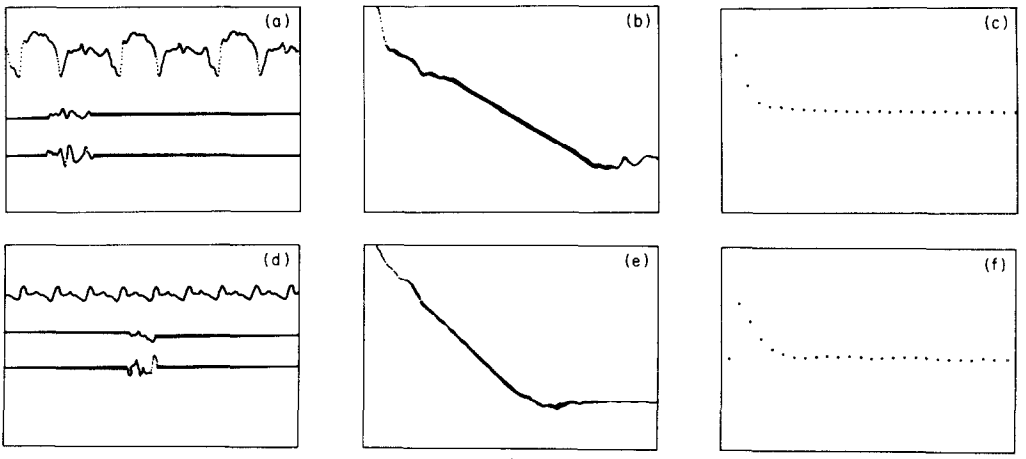

Figure 5. Hot film signal conditioning, autocorrelation and turbulence spectrum Signals at loop (a)–(c) and node (d)–(f) with $I_p = 166$ dB, $f = 2f_0$. (a) and (d) show from top to bottom the complete waveform, conditioned turbulence bursts, and time derivatives of conditioned signals. (b) and (e) Autocorrelation; (c) and (f) turbulence spectrum.

4. DISCUSSION

The problem of an oscillating flow through a pipe has long been studied. Sergeer [2] analyzed the instability of the oscillating boundary layer. He defined a local acoustic Reynolds number,

$$Re_{ac} = u\delta/\nu, \tag{1}$$

where $\delta = \nu/\pi f$ is the oscillating boundary layer thickness, ν is the kinematic viscosity and u is the axial velocity. Sergeer predicted that there can be a transition to turbulence with the critical acoustic Reynolds numbers at about 500. Von Kerczek and Davies [8] studied the oscillating boundary layer based on an energy consideration and stated that turbulence cannot occur for $Re_{ac} < 19$. In view of these theoretical predictions, Merkli and Thomann [3] conducted a series of experiments, utilizing a flow visualization technique, and found that transition to turbulence in an oscillatory flow through a pipe is indeed feasible. By using the oscillational boundary layer thickness $\nu/2\pi f$ as a rough estimation of δ, we found that Re_{ac} has values ranging from 70 to 140, the same order of magnitude as that obtained by Merkli and Thomann.

Once turbulent bursts appeared, measurements were made at locations corresponding to loops and nodes, and the signals were then analyzed (as described in the previous section). From the characteristics of the turbulence, (e.g., power spectral density, r.m.s. values of turbulent velocity, autocorrelation), the Taylor microscale (λ), the integral scale (l), the rate of energy dissipation (ε), the Kolmogorov microscale (η) and the time scale (τ) at different locations, for $f = 684$ Hz and $I_p = 166$ dB, were estimated and the values obtained are shown in Table 1. To check consistency, $\tilde{u}$, λ and η were double checked from the power spectral density. Their corresponding values $\tilde{u}_*$, λ_* and η_* are also given in Table 1. It is seen that they all fall in the same range and are thus consistent. In estimating ε, Batchelor's [9] relation for isotropic turbulence was used:

$$\varepsilon = 15\nu\overline{[\partial u/\partial x]^2} = 15\nu[\tilde{u}/\lambda]^2. \tag{2}$$

To test the validity of the assumption of isotropy, four turbulent spectra F were plotted against the frequency f_t of the turbulence under several different conditions, as shown

TABLE 1

Estimated turbulent characteristics at loop center, loop edge, node center and node edge

	$\tilde{u}$ (m/s)	u_* (m/s)	$\sqrt{(\overline{\partial \tilde{u}/\partial t^2})}$ (10^6 cm/s^2)	λ (mm)	λ_* (mm)	l (cm)	ε (10^6 cm^2/s^3)	η (μm)	η_* (μm)	τ (10^{-4} s)
Loop center	3·0	3·3	2·4	1·8	6·2	1·7	6·5	48	76	1·5
Loop edge	2·8	4·4	2·9	1·3	1·1	2·2	9·8	43	102	1·2
Node center	3·5	3·7	6·2	0·8	0·6	3·2	45	29	101	0·6
Node edge	5·6	5·5	7·2	1·1	1·5	2·8	59	28	178	0·5

in Figure 6. Under regression analysis these curves show that in the inertial subrange their slopes s are $-1{\cdot}6$, $-1{\cdot}8$, $-1{\cdot}9$, $=2{\cdot}1$ with an average of $-1{\cdot}84$. Compared with the theoretical result of $s = -5/3$ for ideal isotropic turbulence, the deviation is approximately 10%. This indicates that equation (2) is probably a good approximation. Physically this result is not surprising as mixing is very effective in turbulence. Furthermore, turbulence is also characterized by its random behavior. Although large eddies may not be effective enough in removing the anisotropy and inhomogeneity, at sufficiently small scale the rapid mixing and the random nature of the turbulence would completely remove the sense of direction. Consequently, isotropy is achieved.

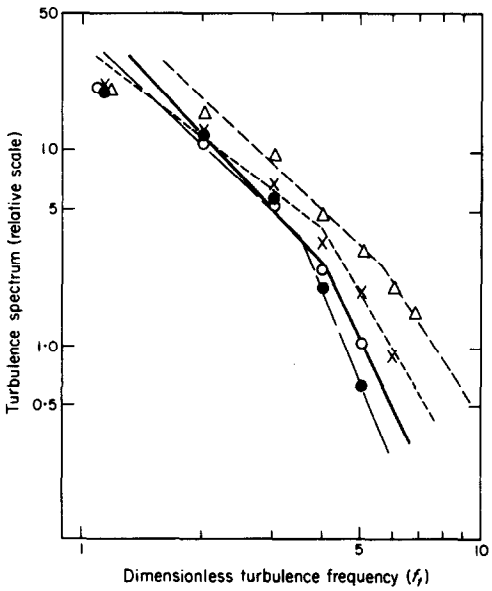

Figure 6. Turbulence spectrum versus dimensionless frequency $f_t = f/200$ at loop and node. Short-dashed lines show the best fitting result at node, for $I_p = 166$ dB, resonance frequency $f_{res} = 3f_0$. The slope is $s = -1{\cdot}6$ in the inertial subrange. Solid lines are at node, $I_p = 166$ dB, $f_{res} = 4f_0$, $s = -2{\cdot}1$. Dashed lines are at loop, $I_p = 166$ dB, $f_{res} = 3f_0$, $s = -1{\cdot}8$. Long-dashed lines are at loop, $I_p = 164$ dB, $f_{res} = f_0$, $s = -1{\cdot}9$. - - - ×, Node 1; —— ●, node 2; - - - △, loop 1; — — ○, loop 2.

Another point in connection with Figure 6 which should be clarified is that in relating F to f_t, Taylor's frozen-turbulence hypothesis was used (see also Figures 5(a) and (d)). As the ratio $\tilde{u}/U$ is usually of the order of 10^{-1} to 10^{-2}, we feel fairly safe in stating that this hypothesis is valid.

In discussing the frequency and intensity dependence of the turbulent velocity, for the sake of clarity, $\tilde{u}$ is used as the measure of the turbulent velocity. In Figure 7 $\tilde{u}$ (at loop and node) is plotted versus I_p. The graphs show that $\log \tilde{u}$ and $\log I_p$ have a linear relationship with the slope

$$\mathrm{d}(\log \tilde{u})/\mathrm{d}(\log I_p) = 1/2. \tag{3}$$

This result states that, regardless of the location,

$$\tilde{u} \propto I_p^{1/2} \tag{4}$$

for acoustically induced turbulence.

The frequency dependence of $\tilde{u}$ is shown in Figure 8. From the wildly scattered pattern of $\tilde{u}$, it seems there is no definite relationship between $\tilde{u}$ and f— or, rather, $\tilde{u}$ is insensitive to f.

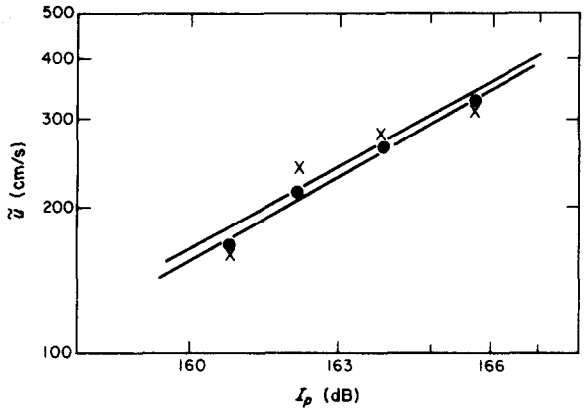

Figure 7. Intensity effect of turbulence rms turbulent velocity $\tilde{u}$ on $I_p^{1/2}$. ×, Loop; ●, node.

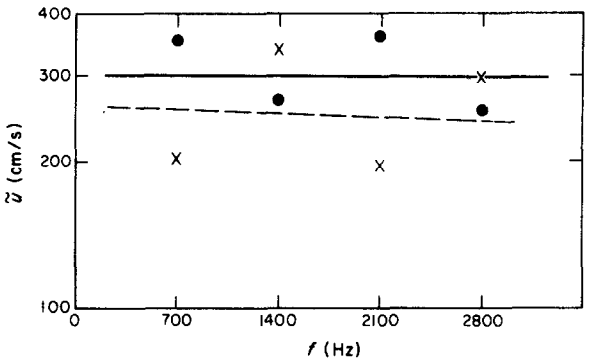

Figure 8. Frequency effect of turbulence. $\tilde{u}$ is plotted against f. Widely scattered pattern shows turbulence is insensitive to frequency variation. ×, Loop; ●, node.

These results seem to suggest that, although the acoustically induced turbulence originated from the boundary layer, once the turbulence occurs it completely forgets its past history and is then driven only by the applied acoustic field.

5. CONCLUSIONS

Acoustically induced turbulence was experimentally studied by using hot film anemometry and the following results were obtained.

(a) Turbulence in a resonance tube can occur only when the sound pressure level passes a certain threshold value. The critical sound pressure level I_p for turbulence is $\sim$160 dB for the experiment performed.

(b) Signals obtained at a loop and a node are different in shape. At a loop the waveform has two shock–response peaks per period. At a node, the waveform is more sawtooth-like with one peak per period. This indicates a position dependence of the shock wave formation.

(c) Isotropy of the turbulence was checked by plotting the spectrum F against the dimensionless frequency f_t of the turbulence. In the inertial subrange it is found that $F \propto f_t^s$, with an average $s = -1{\cdot}84$, which is close to the theoretical value of $-5/3$.

(d) The r.m.s. turbulent velocity $\tilde{u}$ has a functional dependence on I_p of $\tilde{u} \propto I_p^{1/2}$, regardless of location, but is insensitive to variations of f.

(e) The Reynolds number Re_{ac} in the form given by Merkli is found to be between 70 and 140 at the onset of acoustically induced turbulence.

REFERENCES

1. R. T. BEYER 1965 *Nonlinear Acoustics, Physical Acoustics Series.* New York: Academic Press.
2. S. I. SERGEER 1966 *Fluid Dynamics* **1**, 121–132. Fluid oscillations in pipes at moderate *Re*-numbers.
3. P. MERKLI and H. THOMANN 1975 *Journal of Fluid Mechanics* **70**, 567–576. Transition to turbulence in oscillating pipe flow.
4. R. A. SALINGER and G. E. HUDSON 1960 *Journal of the Acoustical Society of America* **32**, 961–969. Periodic shock waves in resonating gas columns.
5. W. CHESTER 1964 *Journal of Fluid Mechanics* **18**, 44. Resonant oscillations in closed tubes.
6. B. T. CHU and S. J. YING 1963 *The Physics of Fluids* **6**, 1625–1638. Thermally driven nonlinear oscillations in a pipe with traveling shock waves.
7. S. TEMKIN 1968 *The Physics of Fluids* **11**, 960–974. Nonlinear gas oscillations in a resonant tube.
8. C. VON KERCZEK and S. H. DAVIES 1972 *Studies in Applied Mathematics* **2**, 239–247. The stability of oscillatory Stokes layers.
9. G. K. BATCHELOR 1956 *Theory of Homogeneous Turbulence.* London: Cambridge University Press.

APPENDIX: NOMENCLATURE

F	turbulent spectrum
f	acoustic frequency
f_{res}	resonant frequency
f_t	dimensionless turbulent frequency
f_0	specific resonant frequency (= 680 Hz)
I_p	sound pressure level, *re* 20 μPa
k	wave number
l	Euler integral scale
Re_{ac}	acoustic Reynolds number
s	slope of turbulent spectrum in the inertial subrange
U	oscillational velocity of the acoustic field
u	root mean square turbulent velocity
u_*	root mean square turbulent velocity estimated from turbulent power spectrum density
Δf	frequency range
δ	characteristic length scale
ε	time rate of turbulent energy dissipation per unit mass
η	Kolmogorov length scale
η_*	Kolmogorov length scale estimated from turbulent power spectral density
λ	Taylor microscale
λ_*	Taylor microscale estimated from turbulent power spectral density
ν	kinematic viscosity
τ	Kolmogorov microscale, time